SANS Determination of Chain Conformation in Perpendicular-Aligned Undecablock Copolymer Lamellae

Lifeng Wu,[†] Timothy P. Lodge,[†,‡] and Frank S. Bates*[,†]

Department of Chemical Engineering and Materials Science and Department of Chemistry, University of Minnesota, Minneapolis, Minnesota 55455

Received August 16, 2005; Revised Manuscript Received November 2, 2005

ABSTRACT: Small-angle neutron scattering (SANS) measurements were conducted on mixtures of deuterated and normal compositionally symmetric CPCPCPCPCPC (or $(CP)_{10}$) undecablock copolymers, containing poly(cyclohexylethylene) (C) and poly(ethylene-*alt*-propylene) (P) blocks. Deuterium labeling was achieved by hydrogenating and deuterating the same $(SI)_{10}$ undecablock precursor. SANS patterns obtained from shear-aligned specimens could be separated into molecular scattering and domain scattering. The overall undecablock radii of gyration, extracted using the Guinier relation, indicate that the undecablock chains adopt a three-dimensional random walk in the perpendicular-arranged lamellae.

Introduction

One of the fascinating features of multiblock copolymers is the bridging and looping conformations for internal blocks (Figure 1a,b). Some theoretical efforts have been undertaken to evaluate the population of bridges in equilibrium multiblock lamellae.[1−11] In particular, Matsen predicted that the fraction of bridging blocks in ABA triblocks is about 40% based on self-consistent mean-field theory calculations,[4−6] while Drolet and Fredrickson showed that varying the ratio of end to center block molecular weight in ABABA pentablock copolymers shifts the fraction of bridged center blocks.[12] Previous experimental results involving either dielectric relaxation[13−15] or microdomain spacing[16,17] of lamellar multiblock copolymers are broadly consistent with these mean-field theory predictions. Recently, an interesting interplay between molecular conformation and lamellae alignment was revealed for a lamellar SISISIS heptablock copolymer under shear flow,[18] where S denotes poly(styrene) and I denotes poly(isoprene). Certain shear conditions aligned this polymer to two distinct states of orientations: the "parallel" arrangement with the lamellae parallel to the plane of shear ($\mathbf{v} - \nabla \times \mathbf{v}$) (Figure 1a) and the "perpendicular" form where the lamellae are aligned perpendicular to the plane of shear with the lamellae normal along the vorticity ($\nabla \times \mathbf{v}$) direction (Figure 1b). Interestingly, the parallel-aligned SISISIS exhibited extensive delamination in the poly(isoprene)-selective solvent tetradecane, attributed to predominant looping conformations in the lamellae (Figure 1a); in contrast, the perpendicular-aligned lamellae remain nearly intact under the same swelling conditions, associated with a considerable population of bridging conformations in the microdomains. Furthermore, even the "forbidden" transverse orientation with the layer normal along the shear direction was observed by abrupt cessation of shearing in CECEC pentablocks[19] and by solution extrusion of SBSBS pentablocks at high shear rates.[20] This suggests that very strong flow might stretch multiblock chains along the flow direction, followed by reordering in the transverse orientation upon cessation of flow. All these results indicate that chain conformation plays an important role in determining lamellar alignment of multiblock copolymers under shear flow.

Unfortunately, it is very difficult to identify the conformational state of individual block copolymer chains within the ordered microdomains. Dielectric relaxation spectroscopy has been one documented method to determine the fraction of bridges, but based on some tentative assumptions.[13−15] Even worse, the dielectric loss cannot distinguish the contribution between bridges and knotted loops; the latter might be significant in ordered multiblock lamellae. In contrast, small-angle neutron scattering (SANS) offers a better chance to extract information related to the single-chain conformation, although deuterium labeling and extraction of molecular scattering can be challenging. The radius of gyration, R_g, of polymer chains can be extracted from the molecular scattering for mixtures of a protonated polymer and its deuterated counterpart, based on the Guinier relation[21]

$$I_m = I_0 \exp(-q^2 R_{g,j}^2)$$

where I_m is the intensity from molecular scattering, I_0 is a prefactor depending on both composition and scattering contrast of the mixture, q ($= (4\pi\lambda^{-1}) \sin(\theta/2)$) is the magnitude of scattering wavevector with wavelength λ and scattering angle θ, and $R_{g,j}$ is the radius of gyration with respect to the plane perpendicular to the **j** direction. The overall radius of gyration $R_g = \sqrt{3}R_{g,j}$ for isotropically distributed polymer chains. SANS measurements have demonstrated Gaussian (unperturbed) chain conformations for amorphous polymers in concentrated solutions and in melts.[22,23] For lamellar diblock copolymers, however, chains are stretched along the lamellae normal;[24−31] as a result, copolymer chains shrink parallel to the interface with the ratio of 0.6−0.7 relative to the unperturbed chain dimension.[24,26,27] For symmetric triblock copolymers, it has been found that the R_g of the middle block is closer to its unperturbed size, with a ca. 10% deviation.[32,33] Chain dimension measurements have not been documented for multiblock copolymers beyond diblocks and triblocks. Figure 1b shows two extreme undecablock chain conformations in the perpendicular-arranged lamellae: one with a fully extended conformation and the other adopting a three-dimensional random walk. As a first approximation, the aspect ratio of $R_{g,\nabla\times v}$ to $R_{g,\nabla v}$ is 10 for the all-bridging configuration and is 1 for the random chain conformation. Parts c and d of Figure 1 illustrate anticipated

† Department of Chemical Engineering and Materials Science.
‡ Department of Chemistry.
* Author for correspondence: e-mail bates@cems.umn.edu.

10.1021/ma0518104 CCC: $33.50
Published on Web 12/06/2005

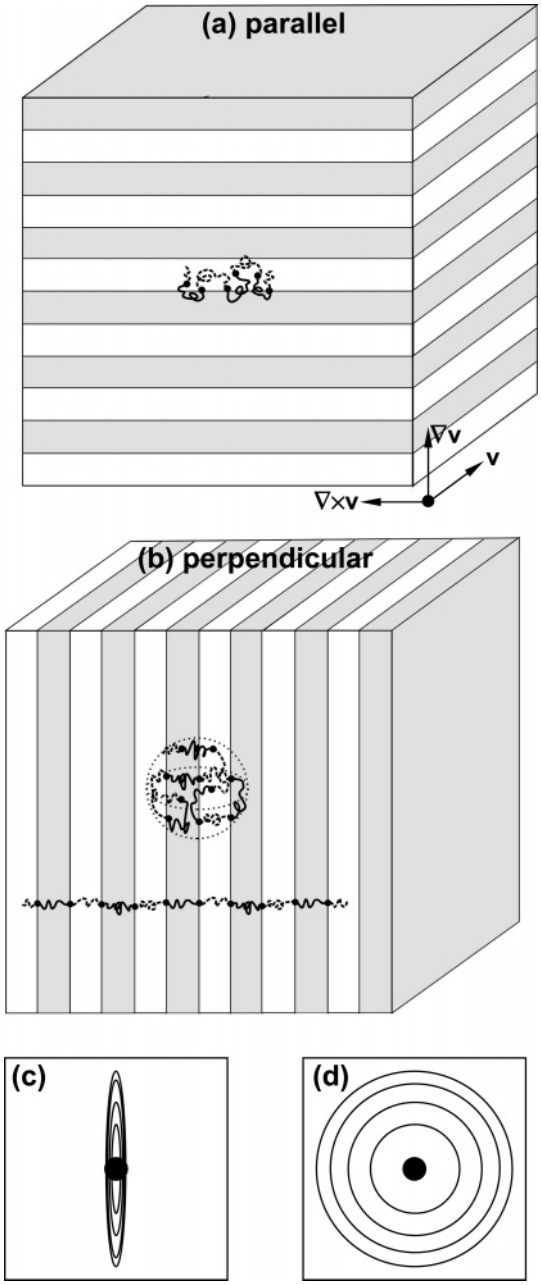

Figure 1. Coordinate system for (a) parallel and (b) perpendicular lamellae alignment under reciprocating shear. A heptablock copolymer molecule with all-looping conformation is shown in the parallel-arranged lamellae, based on the previous swelling experiments,[18] whereas a fully extended and a three-dimensional randomly walked undecablock chains are illustrated in the perpendicular arrangement. (c) and (d) illustrate anticipated SANS contour patterns for fully extended and a three-dimensional randomly walked undecablock chains, respectively.

SANS contour patterns for chain conformations with the aspect ratios of 10 and 1, respectively.

In this study, we employed a saturation scheme to accomplish the deuterium labeling for a compositionally symmetric SISISISISIS (or $(SI)_{10}$) undecablock copolymer. SANS measurements were conducted on mixtures of deuterated and protonated CPCPCPCPCPC (or $(CP)_{10}$) undecablock copolymers; here C denotes poly(cyclohexylethylene) and P denotes poly(ethylene-*alt*-propylene), derived from saturation of S and I, respectively. The overall undecablock radii of gyration were extracted using the Guinier relation to reveal the state of chain conformations in the perpendicular-aligned lamellae.

Experimental Section

Linear SISISISISIS was prepared as previously described[34] by sequential anionic polymerization of styrene and isoprene leading to a living $SISISI^-,Li^+$ hexablock that was coupled with α,α′-dibromo-*p*-xylene. Size exclusion chromatography (SEC) analysis indicated a coupling efficiency of 82%. The overall number-average molecular weight (M_n) of this polymer is 1.63×10^5 g mol^{-1}, with polydispersity index $M_w/M_n < 1.07$. An overall S volume fraction of $f_S = 0.51$ (calculated from the molar composition established by ^{1}H NMR, using densities $\rho_S = 1.04$ g cm^{-1} and $\rho_I = 0.913$ g cm^{-1}) was achieved by making the S end blocks half the size of the internal S and I blocks. This undecablock molecule can also be viewed as a decamer of symmetric SI diblock repeat units, i.e., $(SI)_{10}$. It should be noted that in several previous studies of multiblock $(SI)_n$ copolymers the end S blocks had the same length as the internal S blocks, leading to a total composition and domain spacing that depended significantly on n.[2,3,16,17,35,36] $(SI)_{10}$ was hydrogenated and deuterated to achieve $(CP)_{10}$ and *d*-$(CP)_{10}$, respectively, using the heterogeneous Pt−Re/SiO_2 catalyst. Complete saturation was achieved for both hydrogenated and deuterated products based on the ^{1}H NMR results. SEC traces indicate that the molecular weight distributions remain unchanged after saturation. The densities were measured to be 0.9106 g/cm^3 for $(CP)_{10}$ and 0.9618 g/cm^3 for *d*-$(CP)_{10}$ using a density gradient column made of ethylene glycol and 2-propanol. Because both S and I blocks simultaneously experience saturation reactions accompanied by isotopic exchange, the deuterium per repeat unit (DPR) cannot be determined for particular blocks on the basis of the density results. However, the value averaged over all C and P repeat units is 0.78 deuterium per carbon atom for *d*-$(CP)_{10}$. The order−disorder transition temperature (T_{ODT}) is 227 and 223 °C for $(CP)_{10}$ and *d*-$(CP)_{10}$, respectively, located rheologically with an isochronal temperature scan measured with 1% strain amplitude and a frequency of 1 rad/s while heating specimens at 1 °C/min.

A volume-based 50/50 mixture of $(CP)_{10}$ and *d*-$(CP)_{10}$ was prepared by dissolution in benzene, followed by the removal of benzene using freeze-drying. This mixture was hot-pressed at 150 °C for 3 min and subsequently annealed at 200 °C overnight to obtain a void-free sample. Perpendicular-aligned samples were prepared under nitrogen using a reciprocating shear device described previously.[37] Each specimen was held between two 2.5 cm × 1.9 cm channel-cut aluminum plates with a thickness of 1 mm. Aluminum tape was used to cover the surfaces of plates in order to easily remove samples after shearing. Each specimen was loaded into the instrument and heated to 250 °C, 25 deg above the T_{ODT}. After 10 min, the sample was cooled to 210 °C and held at this temperature for 30 min. Reciprocating shear was then applied for 5 h with 100% strain amplitude and a shear frequency of 0.01 rad s^{-1}. After processing, the samples were cooled to room temperature and carefully removed from the shear device. An unaligned sample was prepared using the same protocol, except for the imposition of reciprocating shear. To study the chain dimension from the edge view along the vorticity direction ($\nabla \times \mathbf{v}$), the perpendicular-aligned sample was cut parallel to the plane of shear ($\mathbf{v}$)−gradient ($\nabla\mathbf{v}$) to 1 mm wide pieces, which were stacked along the gradient direction and then fixed using epoxy resin. A similar procedure was followed to make an edge-view sample along the shear direction.

The SANS measurements were conducted at room temperature on the NIST/Exxon/University of Minnesota 30 m instrument at the National Institute of Standards and Technology (NIST), with wavelength $\lambda = 0.6$ nm and $\Delta\lambda/\lambda = 0.11$. Raw scattering data were corrected for instrumental sensitivity and normalized using precalibrated secondary standards.[38]

Results and Discussion

Figure 2a−d shows SANS contour patterns at a sample-to-detector distance of 3 m for one unaligned sample and three perpendicular-aligned samples with the neutron beam passing

along the **v**, ∇**v**, and $\nabla \times$ **v** directions, respectively. The integration over the azimuthal angle reduces the data to the one-dimensional form of intensity vs scattering wavevector q. Narrow diffraction peaks located at q^*, $2q^*$, ... indicate a lamellar morphology, with periodic spacing D ($= 2\pi/q^*$) of 17.5 nm for the unaligned sample and 18.0 nm for the perpendicular-aligned sample. Interestingly, the molecular scattering due to the conformational characteristics of deuterium-labeled chains separates very well from the Bragg scattering due to the periodic lamellar domain for this undecablock copolymer. This feature is expected for block copolymers with a large number of blocks because (1) the Bragg scattering mainly depends on the size of diblock unit and therefore is not sensitive to the number of blocks and (2) the molecular scattering depends on the size of individual molecules such that the increase of block number squeezes the molecular scattering toward the center of SANS pattern. In contrast, as reported previously,[25−30] molecular scattering and Bragg scattering overlap to a significant extent for diblock copolymers due to similar sizes between diblock molecules and lamellae thickness, making it difficult to resolve the molecular scattering.

In addition, Figure 2b,c shows slight anisotropy in the molecular scattering. To improve the resolution of molecular scattering, a sample-to-detector distance of 11 m was used to examine the above four samples; the resulting patterns are shown in Figure 2e−h. Isotropic patterns were recorded for the unaligned sample and the perpendicular-aligned sample viewed along the $\nabla \times$ **v** direction, while slightly anisotropic patterns were obtained for the perpendicular-aligned samples viewed along the **v** and ∇**v** directions. Compared to Figure 1c,d, these results indicate copolymer chains essentially walk randomly in the perpendicular-aligned lamellae. In addition, two edge-view samples display asymmetric high-intensity scattering near the beam stop (Figure 2f,h), which was not observed for the other two through-view samples. We attributed this to the reflection from interfaces between stacked small pieces in the edge-view samples.

The radii of gyration were evaluated based on the Guinier relation. To extract the contribution of molecular scattering, the incoherent scattering background should be subtracted from the above SANS data. As a good approximation, the incoherent scattering of blends can be evaluated as the volume-averaged incoherent scattering of pure components. Figure 3 shows the SANS intensity vs q for unaligned pure $(CP)_{10}$, d-$(CP)_{10}$, and a 50/50 $(CP)_{10}/d$-$(CP)_{10}$ mixture at the sample-to-detector distance of 11 m. The deuterated sample exhibits much stronger domain scattering at $q^* = 0.35$ nm^{-1} than the protonated one. This can be associated with larger scattering contrast between deuterium-labeled C and P microdomains for d-$(CP)_{10}$ because the deuteration process leads to larger DPR for C blocks than that for P blocks. In addition, the low-angle scattering is nearly flat for $(CP)_{10}$, which can be associated with the incoherent scattering, whereas the scattering intensity of d-$(CP)_{10}$ increases dramatically as q decreases. This low-q coherent scattering has been observed for other deuterated polymers;[39−42] it can be attributed to particulate impurities such as catalyst residues, voids in glassy C domains, and nonuniform deuterium labeling along the copolymer chain. The first factor can be ruled out because no angular dependence was found for the protonated $(CP)_{10}$, which was made from the same precursor, then purified, and processed identically as d-$(CP)_{10}$. Further, increasing temperature to 120 °C has no perceptible effect on the scattering profile of d-$(CP)_{10}$ in the low q region, indicating that voids play no role here. We therefore attribute this coherent scattering to the nonuniform labeling along the copolymer chain. Balsara et al. reported that the slight difference in deuteration levels among the homopolymer chains can lead to significant coherent patterns in SANS experiments.[39−42] They used the random phase approximation (RPA) theory to calculate the scattering profile for the blend of a protonated polymer and its nonuniformly deuterium-labeled counterpart. They predicted that the scattering of the deuterated component alone is proportional to the variance of the scattering length distribution and the single chain form factor that has a q dependence; with the addition of the protonated counterpart, this contribution is additive to the overall scattering and is proportional to the volume fraction of the deuterated polymer. This indicates that this undesired coherent scattering depends linearly on the blend composition. Because the incoherent scattering also follows a linear mixing rule for the blends, the molecular scattering of the $(CP)_{10}/d$-$(CP)_{10}$ blend can be extracted from the SANS data by subtracting the volume-averaged overall scattering between pure $(CP)_{10}$ and d-$(CP)_{10}$, which is shown as the smooth curve in Figure 3.

Figure 4 shows the Guinier plot of $\ln(I_m)$ vs q^2 for these molecular scattering data, which were circular-averaged for the unaligned sample or sector-averaged along the **v**, ∇**v**, and $\nabla \times$ **v** directions with a $\pm 7.5°$ angle range for the perpendicular-aligned samples. The radii of gyration were evaluated using the least-squares fit for the data within $0.002 \text{ nm}^{-2} \le q^2 \le 0.02 \text{ nm}^{-2}$. For comparison, an arrow identifies $qR_g = 1$ for the unaligned and one aligned sample. Acceptable linear fits were achieved for all these data. For the perpendicular samples, sector-averaged data from different SANS patterns show the same slope along either **v** or $\nabla \times$ **v** direction. As shown in Figure 2f,h, the strong reflection of two edge-view samples overlaps with the low q molecular scattering ($q < 0.1$ nm^{-1}) along the ∇**v** direction such that $R_{g,\nabla v}$ cannot be directly obtained from the data fitting. A careful examination of these two SANS patterns indicates that $R_{g,j}^2$, evaluated from the sector-averaged data along a certain **j** direction, follows an elliptical trajectory with respect to the center. Therefore, $R_{g,\nabla v}^2$ was extrapolated from $R_{g,j}^2$ ($\mathbf{j} \neq \nabla \mathbf{v}$) on these two SANS patterns (Figure 2f,h) and plotted as straight lines on the Guinier plot along the ∇**v** direction in Figure 4.

Table 1 shows the radii of gyration calculated from SANS data for the unaligned and perpendicular-aligned samples. The undecablock chains in the perpendicular-arranged lamellae exhibit a slight deviation from spherical symmetry. The projection of copolymer chains in the **v**−∇**v** plane is nearly isotropic, whereas they extend slightly along the $\nabla \times$ **v** direction with an aspect ratio of 1.15. For this spheroidal chain arrangement, the overall radius of gyration can be calculated as $R_g = \sqrt{R_{g,v}^2 + R_{g,\nabla v}^2 + R_{g,\nabla \times v}^2} = 10.5$ nm, nearly the same as the overall radius of gyration of 10.4 nm for the unaligned sample. In addition, we can compare this chain dimension with the following two random walk models. First, we assume that each undecablock copolymer chain adopts a three-dimensional random walk. The overall mean-square end-to-end distance $\langle h^2 \rangle = \langle h^2 \rangle_C + \langle h^2 \rangle_P$ for copolymer chains. Fetters et al. reported that $\langle h^2 \rangle / M = 3.23 \times 10^{-3}$ and 8.34×10^{-3} nm^2 mol g^{-1} for C and P homopolymers, respectively.[43] For the protonated $(CP)_{10}$ undecablock copolymer, the total C block molecular weight $M_C = 9.19 \times 10^4$ g mol^{-1} and the total P block molecular weight $M_P = 7.81 \times 10^4$ g mol^{-1}. As a result, the overall radius of gyration $R_g = \sqrt{\langle h^2 \rangle / 6} = 12.6$ nm. On the other hand, we can assume that an undecablock chain $(CP)_{10}$ randomly walks 10 steps in a three-dimension space. The step length l can be

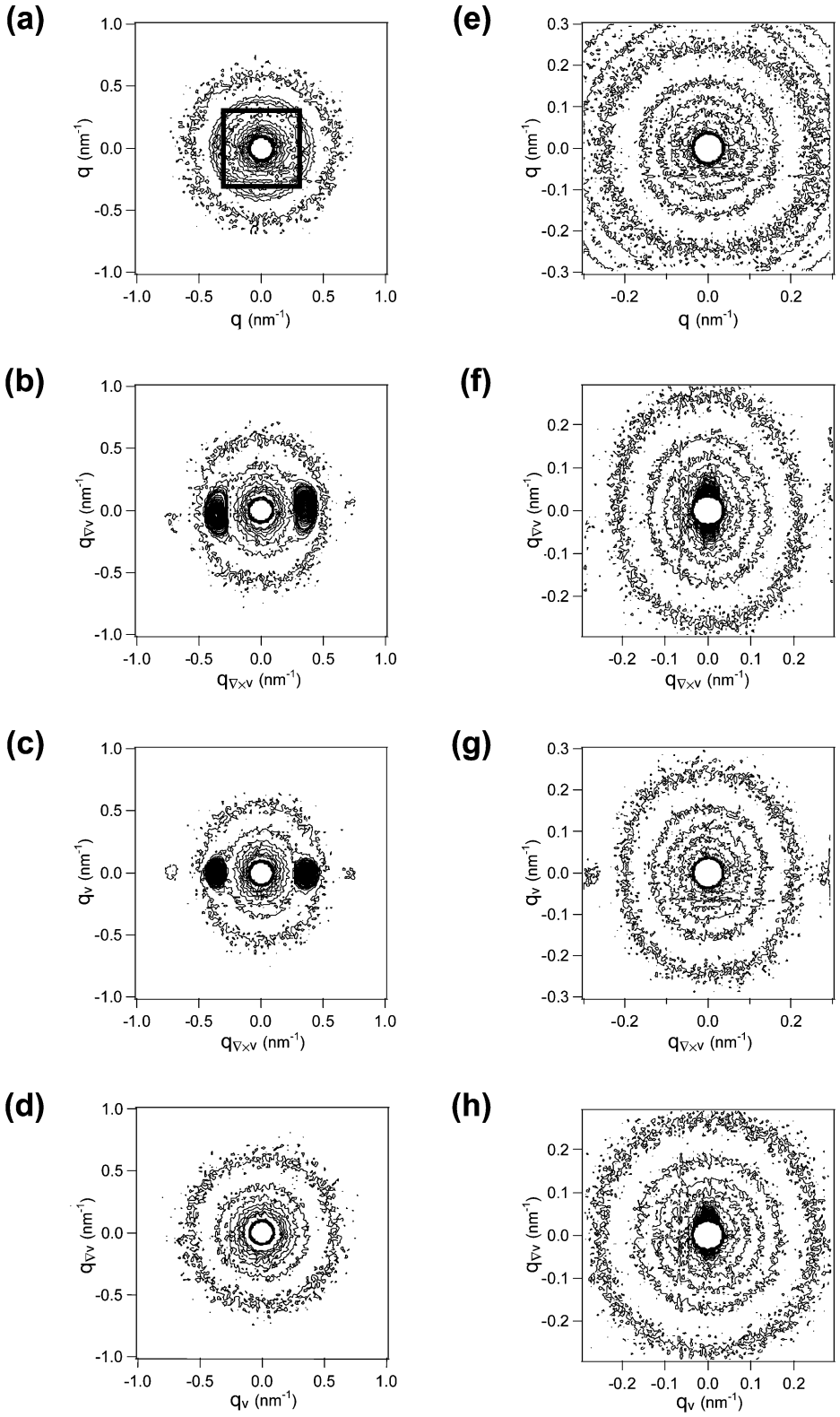

Figure 2. Two-dimensional SANS contour patterns of 50/50 $(CP)_{10}/d$-$(CP)_{10}$ blends for (a) the unaligned state and the perpendicular orientation viewed along the (b) **v**, (c) ∇**v**, and (d) $\nabla \times$ **v** directions at a sample-to-detector distance of 3 m. (e), (f), (g), and (h) are SANS patterns of these four samples, respectively, reexamined at a sample-to-detector distance of 11 m. The square in (a) illustrates the q region in (e) accessed at the sample-to-detector distance of 11 m.

associated with the mean-square-root end-to-end distance $\sqrt{\langle h^2 \rangle}$ of the CP diblock unit. Hashimoto et al. demonstrated that the component of $\sqrt{\langle h^2 \rangle}$ along the lamellae normal is fairly close to $D/2$.[44] As a good approximation, we take $l \approx D/2 = 9.0$ nm for $(CP)_{10}$ and obtain the overall radius of gyration $R_g = \sqrt{\langle h^2 \rangle/6} = \sqrt{10l^2/6} = 11.6$ nm. Therefore, the overall radii of gyration obtained from both random walk models are fairly close to the above SANS results.

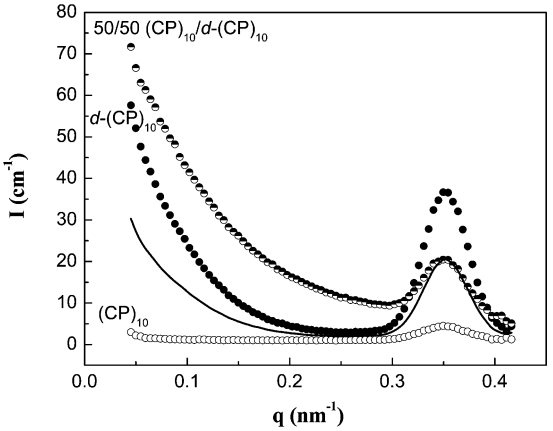

Figure 3. Circular-averaged intensity of neutron scattering as a function of q for the unaligned pure $(CP)_{10}$ and d-$(CP)_{10}$ and the unaligned 50/50 $(CP)_{10}/d$-$(CP)_{10}$ mixture, denoted by open, filled, and partially filled circles, respectively. These samples experienced the same processing history as the aligned 50/50 $(CP)_{10}/d$-$(CP)_{10}$ blends. The measurements were conducted at a sample-to-detector distance of 11 m. The smooth curve illustrates the volume-averaged overall scattering between pure $(CP)_{10}$ and d-$(CP)_{10}$.

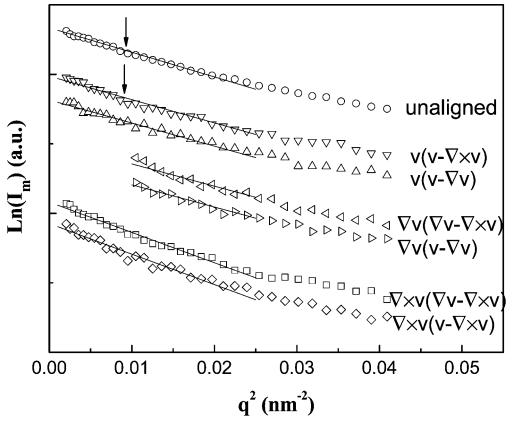

Figure 4. Guinier plot of $\ln(I_m)$ vs q^2 for the circular-averaged data of the unaligned 50/50 $(CP)_{10}/d$-$(CP)_{10}$ sample and the sector-averaged data along the **v**, ∇**v**, and $\nabla \times$ **v** directions for the perpendicular-aligned 50/50 $(CP)_{10}/d$-$(CP)_{10}$ samples. For comparison, an arrow identifies $qR_g = 1$ for the unaligned and one aligned sample. $R_{g,\nabla v}^2$ was extrapolated from $R_{g,j}^2$ ($\mathbf{j} \neq \nabla\mathbf{v}$) on the SANS patterns in Figure 2f,h and plotted as straight lines on the Guinier plot along the ∇**v** direction.

Table 1. Radii of Gyration in the $(CP)_{10}$ Undecablock Lamellae

unaligned R_g (nm)	perpendicular $R_{g,v}$ (nm)	$R_{g,\nabla v}$ (nm)	$R_{g,\nabla\times v}$ (nm)
10.4	5.8	5.7	6.6

These results suggest that undecablock chains arrange essentially randomly with both bridging and looping conformations in the lamellar microdomains; the shear conditions leading to the perpendicular orientation have very little effect on the chain conformations. As proposed in our previous work,[45] to reduce the chain stretching in the perpendicular-arranged lamellae under shear, the copolymer chains can adopt conformations with a two-dimensional random walk in the plane of shear (Figure 5a). This chain conformation can relax back to a nearly three-dimensional random walk upon the cessation of shear (Figure 5b) while maintaining the block junctions at the same domain boundaries. Because this process does not involve a mechanism of block pullout through unfavorable microdomains, a three-dimensional chain conformation can be achieved without paying a high-energy penalty. The slight anisotropy along the $\nabla \times$ **v** direction can be associated with slight chain stretching

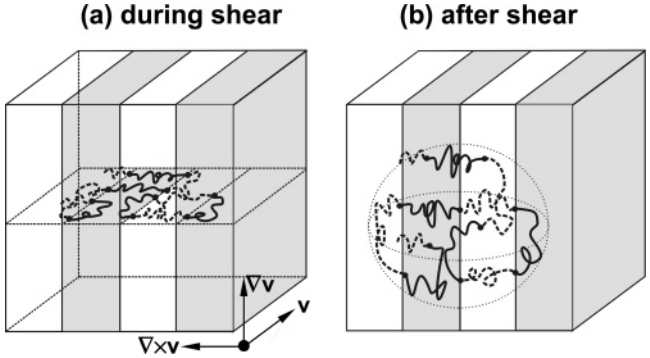

Figure 5. Representative chain conformations of undecablock copolymer in the perpendicular-aligned lamellae (a) during shear and (b) after shear. To reduce the chain stretching, the copolymer chains can adopt conformations with a two-dimensional random walk on the plane of shear in the perpendicular-arranged lamellae under shear; this chain conformation can relax back to a three-dimensional random walk upon the cessation of shear.

of each diblock unit along the normal of lamellae. In contrast, as observed for a parallel-aligned heptablock copolymer, large strain shear tends to induce predominantly looping conformations (Figure 1a).[18] We proposed in the previous paper that this conformation is also a two-dimensional random walk on the plane of shear;[45] however, these conformations cannot return to a three-dimensional random walk after shearing due to a large free energy penalty for transporting chains through segregated microdomains.

These studies have revealed an interesting connection between chain conformation and microdomain alignment under shear flow. Multiblock chains adopt a three-dimensional random walk following perpendicular alignment and a two-dimensional random walk on the plane of shear for the parallel-aligned sample. Besides the swelling behavior we studied previously, the chain conformation should also play an important role in mechanical properties. Mori and co-workers demonstrated that addition of 10−15% CECEC pentablocks into CEC triblocks significantly improves mechanical properties;[46] the enhanced toughness has been associated with the increasing populations of bridging C blocks due to the addition of CECEC. In the future, it will be of interest to examine the difference in mechanical properties between perpendicular and parallel-aligned multiblock copolymers and to correlate it to the molecular conformations in these materials.

Acknowledgment. This research was supported primarily by the MRSEC program of the National Science Foundation under Award DMR-0212302. The authors thank Paul Butler for help with SANS experiments at NIST.

References and Notes

(1) Zhulina, E. B.; Halperin, A. *Macromolecules* **1992**, *25*, 5730.
(2) Zielinski, J. M.; Spontak, R. J. *Macromolecules* **1992**, *25*, 653.
(3) Spontak, R. J.; Zielinski, J. M.; Lipscomb, G. G. *Macromolecules* **1992**, *25*, 6270.
(4) Matsen, M. W.; Schick, M. *Macromolecules* **1994**, *27*, 187.
(5) Matsen, M. W.; Schick, M. *Macromolecules* **1994**, *27*, 7157.
(6) Matsen, M. W. *J. Chem. Phys.* **1995**, *102*, 3884.
(7) Matsen, M. W.; Thompson, R. B. *J. Chem. Phys.* **1999**, *111*, 7139.
(8) Li, B.; Ruckenstein, E. *Macromol. Theor. Simul.* **1998**, *7*, 333.
(9) Huh, J.; Jo, W. H.; ten Brinke, G. *Macromolecules* **2002**, *35*, 2413.
(10) Rasmussen, K. O.; Kober, E. M.; Lookman, T.; Saxena, A. *J. Polym. Sci., Part B: Polym. Phys.* **2002**, *41*, 104.
(11) Thompson, R. B.; Rasmussen, K. O.; Lookman, T. *J. Chem. Phys.* **2004**, *120*, 3990.
(12) Drolet, F.; Fredrickson, G. H. *Macromolecules* **2001**, *34*, 5317.
(13) Watanabe, H. *Macromolecules* **1995**, *28*, 5006.
(14) Watanabe, H.; Tan, H. *Macromolecules* **2004**, *37*, 5118.

(15) Karatasos, K.; Anastasiadis, S. H.; Pakula, T.; Watanabe, H. *Macromolecules* **2000**, *33*, 523.
(16) Smith, S. D.; Spontak, R. J.; Satkowski, M. M.; Ashraf, A.; Lin, J. S. *Phys. Rev. B* **1993**, *47*, 14555.
(17) Smith, S. D.; Spontak, R. J.; Satkowski, M. M.; Ashraf, A.; Heape, A. K.; Lin, J. S. *Polymer* **1994**, *35*, 4527.
(18) Wu, L.; Lodge, T. P.; Bates, F. S. *Macromolecules* **2004**, *37*, 8184.
(19) Vigild, M. E.; Chu, C.; Sugiyama, M.; Chaffin, K. A.; Bates, F. S. *Macromolecules* **2001**, *34*, 951.
(20) Harada, T.; Bates, F. S.; Lodge, T. P. *Macromolecules* **2003**, *36*, 5440.
(21) Guinier, A.; Fournet, G. *Small-Angle Scattering of X-rays*; John Wiley & Sons: New York, 1955.
(22) Cotton, J. P.; Decker, D.; Benoit, H.; Farnoux, B.; Higgins, J.; Jannink, G.; Ober, R.; Picot, C.; Des Cloizeaux, J. *Macromolecules* **1974**, *7*, 863.
(23) Higgins, J. S.; Stein, R. S. *J. Appl. Crystallogr.* **1978**, *11*, 346.
(24) Hadziioannou, G.; Picot, C.; Skoukios, A.; Ionescu, M. L.; Mathis, A.; Duplessix, R.; Gallot, Y.; Lingelser, J. P. *Macromolecules* **1982**, *15*, 263.
(25) Bates, F. S.; Berney, C. V.; Cohen, R. E.; Wignall, G. D. *Polymer* **1983**, *24*, 519.
(26) Hasegawa, H.; Hashimoto, T.; Kawai, H.; Lodge, T. P.; Amis, E. J.; Glinka, C. J.; Han, C. C. *Macromolecules* **1985**, *18*, 67.
(27) Hasegawa, H.; Tanaka, H.; Hashimoto, T.; Han, C. C. *Macromolecules* **1987**, *20*, 2120.
(28) Matsushita, Y.; Nakao, Y.; Saguchi, R.; Mori, K.; Choshi, H.; Muroga, Y.; Noda, I.; Nagasawa, M.; Chang, T. *Macromolecules* **1988**, *21*, 1802.
(29) Matsushita, Y.; Mori, K.; Mogi, Y.; Saguchi, R.; Noda, I.; Nagasawa, M.; Chang, T.; Glinka, C. J.; Han, C. C. *Macromolecules* **1990**, *23*, 4317.
(30) Matsushita, Y.; Mori, K.; Saguchi, R.; Noda, I.; Nagasawa, M.; Chang, T.; Glinka, C. J.; Han, C. C. *Macromolecules* **1990**, *23*, 4387.
(31) Koizumi, S.; Hashimoto, T. *Phys. B* **1995**, *213&214*, 703.
(32) Matsushita, Y.; Nomura, M.; Watanabe, J.; Mogi, Y.; Noda, I.; Imai, M. *Macromolecules* **1995**, *28*, 6007.
(33) Matsushita, Y.; Torikai, N.; Suzuki, J.; Seki, M. *J. Phys. Chem. Solids* **1999**, *60*, 1279.
(34) Wu, L.; Cochran, E. W.; Lodge, T. P.; Bates, F. S. *Macromolecules* **2004**, *37*, 3360.
(35) Spontak, R. J.; Smith, S. D.; Satkowski, M. M.; Ashraf, A.; Zielinski, J. M. In *Studies in Polymer Science: Polymer Solutions, Blends, and Interfaces*; Elsevier: New York, 1992; p 65.
(36) Spontak, R. J.; Smith, S. D. *J. Polym. Sci., Part B: Polym. Phys.* **2001**, *39*, 947.
(37) Koppi, K. A. Shear Orientation of Diblock Copolymer Melts. Ph.D. Thesis, University of Minnesota, 1994.
(38) Wignall, G. D.; Bates, F. S. *J. Appl. Crystallogr.* **1987**, *20*, 28.
(39) Bates, F. S.; Fetters, L. J.; Wignall, G. D. *Macromolecules* **1988**, *21*, 1086.
(40) O'Reilly, J. M.; Teegarden, D. M.; Wignall, G. D. *Macromolecules* **1985**, *18*, 2747.
(41) Schelten, J.; Wignall, G. D.; Ballard, D. G. H. *Polymer* **1974**, *15*, 682.
(42) Balsara, N. P.; Lohse, D. J.; Graessley, W. W.; Krishnamoorti, R. *J. Chem. Phys.* **1994**, *100*, 3905.
(43) Fetters, L. J.; Lohse, D. J.; Richter, D.; Witten, T. A.; Zirkel, A. *Macromolecules* **1994**, *27*, 4639.
(44) Hashimoto, T.; Shibayama, M.; Kawai, H. *Macromolecules* **1980**, *13*, 1237.
(45) Wu, L.; Lodge, T. P.; Bates, F. S. *J. Rheol.* **2005**, *49*, 1231.
(46) Mori, Y.; Lim, L. S.; Bates, F. S. *Macromolecules* **2003**, *36*, 9879.

MA0518104